Original Article

Automated volumetric and statistical shape assessment of cam-type morphology of the femoral head-neck region from clinical 3D magnetic resonance images

Jessica M. Bugeja[1,2]^, Ying Xia[2], Shekhar S. Chandra[1], Nicholas J. Murphy[3,4], Jillian Eyles[3,5], Libby Spiers[6], Stuart Crozier[1], David J. Hunter[3,5], Jurgen Fripp[2], Craig Engstrom[7]

[1]School of Information Technology and Electrical Engineering, The University of Queensland, Brisbane, Australia; [2]Australian e-Health Research Centre, Commonwealth Scientific and Industrial Research Organisation, Health and Biosecurity, Herston, Australia; [3]Kolling Institute of Medical Research, Institute of Bone and Joint Research, University of Sydney, Sydney, Australia; [4]Department of Orthopaedic Surgery, John Hunter Hospital, Newcastle, Australia; [5]Department of Rheumatology, Royal North Shore Hospital, St Leonards, Australia; [6]Centre for Health, Exercise and Sports Medicine, Department of Physiotherapy, University of Melbourne, Melbourne, Australia; [7]School of Human Movement Studies, The University of Queensland, Brisbane, Australia

Contributions: (I) Conception and design: JM Bugeja, Y Xia, SS Chandra, S Crozier, J Fripp, C Engstrom; (II) Administrative support: NJ Murphy; (III) Provision of study materials or patients: J Eyles, L Spiers, NJ Murphy, DJ Hunter; (IV) Collection and assembly of data: J Eyles, L Spiers, NJ Murphy, DJ Hunter; (V) Data analysis and interpretation: JM Bugeja, Y Xia, SS Chandra, J Fripp, C Engstrom; (VI) Manuscript writing: All authors; (VII) Final approval of manuscript: All authors.

Correspondence to: Jessica M. Bugeja, BEng (Hons). School of Information Technology and Electrical Engineering, The University of Queensland, St Lucia, Brisbane, QLD 4072, Australia. Email: jessica.bugeja@uq.net.au.

Background: Femoroacetabular impingement (FAI) cam morphology is routinely assessed using manual measurements of two-dimensional (2D) alpha angles which are prone to high rater variability and do not provide direct three-dimensional (3D) data on these osseous formations. We present CamMorph, a fully automated 3D pipeline for segmentation, statistical shape assessment and measurement of cam volume, surface area and height from clinical magnetic resonance (MR) images of the hip in FAI patients.

Methods: The novel CamMorph pipeline involves two components: (I) accurate proximal femur segmentation generated by combining the 3D U-net to identify both global (region) and local (edge) features in clinical MR images and focused shape modelling to generate a 3D anatomical model for creating patient-specific proximal femur models; (II) patient-specific anatomical information from 3D focused shape modelling to simulate 'healthy' femoral bone models with cam-affected region constraints applied to the anterosuperior femoral head-neck region to quantify cam morphology in FAI patients. The CamMorph pipeline, which generates patient-specific data within 5 min, was used to analyse multi-site clinical MR images of the hip to measure and assess cam morphology in male (n=56) and female (n=41) FAI patients.

Results: There was excellent agreement between manual and CamMorph segmentations of the proximal femur as demonstrated by the mean Dice similarity index (DSI; 0.964±0.006), 95% Hausdorff distance (HD; 2.123±0.876 mm) and average surface distance (ASD; 0.539±0.189 mm) values. Compared to female FAI patients, male patients had a significantly larger median cam volume (969.22 *vs.* 272.97 mm^3, U=240.0, P<0.001), mean surface area [657.36 *vs.* 306.93 mm^2, t(95)=8.79, P<0.001], median maximum-height (3.66 *vs.* 2.15 mm, U=407.0, P<0.001) and median average-height (1.70 *vs.* 0.86 mm, U=380.0, P<0.001).

Conclusions: The fully automated 3D CamMorph pipeline developed in the present study successfully segmented and measured cam morphology from clinical MR images of the hip in male and female patients with differing FAI severity and pathoanatomical characteristics.

^ ORCID: 0000-0003-3631-969X.

Keywords: Hip joint; cam-type femoroacetabular impingement syndrome (cam-type FAI syndrome); statistical shape modelling; magnetic resonance imaging (MRI)

Submitted Apr 07, 2022. Accepted for publication Jul 15, 2022.
doi: 10.21037/qims-22-332
View this article at: https://dx.doi.org/10.21037/qims-22-332

Introduction

Cam-type femoroacetabular impingement (FAI) syndrome is characterised by an abnormal asphericity of the femoral head which predisposes to impingement at the anterosuperior acetabular rim and is frequently associated with pain during manoeuvres involving internal hip rotation (1,2). In clinical investigations, cam morphology is commonly assessed using techniques including computerised tomography (CT) or magnetic resonance imaging (MRI) whereby a planar projection, from anterosuperior and/or anterior slices of the femoral head-neck region, is used to calculate a two-dimensional (2D) alpha angle to evaluate femoral head asphericity in patients with suspected FAI (3,4). An alpha angle of greater than 55° is routinely considered indicative of a cam formation although higher thresholds have been proposed with respect to increased specificity of symptomatic FAI (5-7). Currently, the alpha angle is the most commonly used index of cam morphology in hip arthroscopic surgery (8), although it has moderate to poor inter- and intra-reader reliabilities (9) and these 2D measurements do not provide direct geometric data on cam dimensions (e.g., volume, surface area, height) for evaluating the specific morphometric characteristics of these osseous formations.

The development of a fully automated three-dimensional (3D) approach for the assessment of cam morphology, particularly from clinical magnetic resonance (MR) images, to provide fast, robust analyses using deep learning methods has the potential to improve pre- and post-intervention quantitative assessments in patients with FAI (10). We present CamMorph, a fully automated 3D pipeline developed to extract cam morphology from clinical MR images of the hip in FAI patients. The CamMorph pipeline, which generates patient-specific data within 5 min, was used to analyse clinical MR images of the hip to examine cam morphology in FAI patients from the multi-site Australian FASHIoN trial (11).

CamMorph addresses the challenging task of automated segmentation and measurement of cam morphology from clinical 3D MR images in FAI patients acquired on different MR systems and exhibiting varying imaging aspects such as proximal femur coverage, image artefacts and contrast characteristics. In the present study, CamMorph was used to extract cam morphology for volume, surface area and height calculations for a sexual dimorphism comparison of cam morphology between male and female patients with differing FAI severity and pathoanatomical characteristics. We present the following article in accordance with the MDAR reporting checklist (available at https://qims.amegroups.com/article/view/10.21037/qims-22-332/rc).

Methods

The study was conducted in accordance with the Declaration of Helsinki (as revised in 2013). Three datasets of hip MR images were used in the current study. Dataset A (12) and B (13) were used in model training and algorithm development for an automated 3D cam segmentation and assessment pipeline (CamMorph). Dataset C (11), consisting of a clinical MR dataset collected in the Australian FASHIoN trial, was used for dedicated measurement of cam volume, surface area and height in FAI patients using the developed automated 3D CamMorph pipeline. In the present study, the CamMorph measurements of cam volume, surface area, maximum- and average-height were compared between male and female patients.

Training and algorithm development in Datasets A and B

Dataset A, containing 3D true fast imaging with steady-state precession (true-FISP) unilateral hip images with manual bone labels of the proximal femur and acetabulum from 56 asymptomatic volunteers (12), was used for the training of 3D U-net networks to segment the proximal femur volume in the present work.

Dataset B, containing bone surfaces of the proximal femur reconstructed from bilateral water-excited 3D double echo steady state (DESS) hip MR images (13), was used for

focused shape model (FSM) (14) creation in the present work with *a-priori* focus on the femoral head-neck area to enable targeted shape assessment of cam morphology in this clinical region of interest (ROI) for proximal femur segmentation and simulation of a 'healthy' femur bone model through cam morphology relaxation (discussed in later sections).

CamMorph application in Dataset C (Australian FASHIoN MR Dataset)

Dataset C, consisting of baseline MR examinations of the affected hip joint in 97 patients with FAI (56 males, 41 females, aged 16–63 years) from the Australian FASHIoN trial (11), was used for the dedicated measurement of cam volume, surface area and height using the developed automated 3D CamMorph pipeline. All patients recruited for the FASHIoN trial presented with hip pain (assessed using the short form-12, international hip outcome tool and hip osteoarthritis outcome score), radiographic signs of cam and/or pincer morphology (alpha angle of >55° and/or lateral centre edge angle >40° or further radiographic pincer morphology signs such as a positive cross-over sign) and had a surgical opinion that the patient would benefit from arthroscopic hip surgery. For further information on patient recruitment, treatment groups, inclusion and exclusion criteria refer to Murphy *et al.* (11). The baseline MR images in the multi-site FASHIoN study were acquired on various clinical 3T systems (Siemens Prisma, Siemens Skyra, Phillips Ingenia) with a 3D T2-weighted true-FISP sequence [repetition time: 10.2 ms, echo time: 4.3 ms, weighted average image spacing (voxel size varied in this multi-site study): 0.644×0.644×0.668 mm^3, field of view (FOV): 16×16 cm, matrix size: 256×256]. The true-FISP sequence, as used in the Australian FASHIoN trial, can be used for evaluations of hip joint cartilage health and comparisons between MR and X-ray features using the Hip Osteoarthritis MR imaging Scoring System and Hip2Norm software (11).

Proximal femur segmentation analyses

Manual segmentations of the proximal femur from MR examinations of randomly selected patients (n=44) in the FASHIoN study (Dataset C) were used to assess the automated segmentations obtained from a 3D U-net only and a 3D U-net + FSM approach as used in the final CamMorph pipeline. The manual segmentations of the proximal femur (femoral head, neck and proximal shaft) were performed by JMB under expert guidance from an analyst with 20 years of experience (CE). CE reviewed each manual segmentation for quality assurance purposes. These manual segmentations were compared to the automated segmentations using Dice similarity index (DSI), 95% Hausdorff distance (HD) and average surface distance (ASD) values. The equations for these comparative measures are listed below, where A denotes the set of automatically segmented voxels and M denotes the set of manually segmented voxels:

$$DSI(A,M) = \frac{2|A \cap M|}{|A| + |M|} \quad [1]$$

$$HD(A,M) = \max\left(h(A,M), h(M,A)\right) \quad [2]$$

Where $h(A, M)$ is the directed HD and is given by:

$$h(A,M) = \max_{a \in A} \min_{m \in M} \|a - m\| \quad [3]$$

The 95% HD was used in this study, rather than the maximum HD {refer to Eq. [2]} based on the sensitivity of this latter measurement to outliers (15).

$$ASD(A,M) = \max\left(d(A,M),\ d(M,A)\right) \quad [4]$$

Where $d(A, M)$ is the directed average HD and is given by:

$$d(A,M) = \frac{1}{N} \sum_{a \in A} \min_{m \in M} \|a - m\| \quad [5]$$

CamMorph pipeline

Figure 1 provides an overview of the two central components involved in the development of the automated CamMorph segmentation and volumetric analysis pipeline including: component 1 consisting of an initial proximal femur bone 3D U-net segmentation computed on unilateral 3D true-FISP MR images (*Figure 1A*) and component 2 consisting of cam morphology segmentation for calculation of cam volume, surface area and height. The 3D U-net segmentation approach, used for automated bone segmentation of the proximal femur as per component 1 (*Figure 1B*), was modified from Çiçek *et al.* (16). The calculation of cam volume, surface area and height, as per component 2 (*Figure 1C-1F*), starts with a femur bone fitting to the U-net segmentation using femoral bone initialization as per Nishii *et al.* (17), refined with FSM and atlas-based image registration (*Figure 1C*). Subsequently, a simulated 'healthy' bone model is generated for each individual patient using FSM methods focused on the

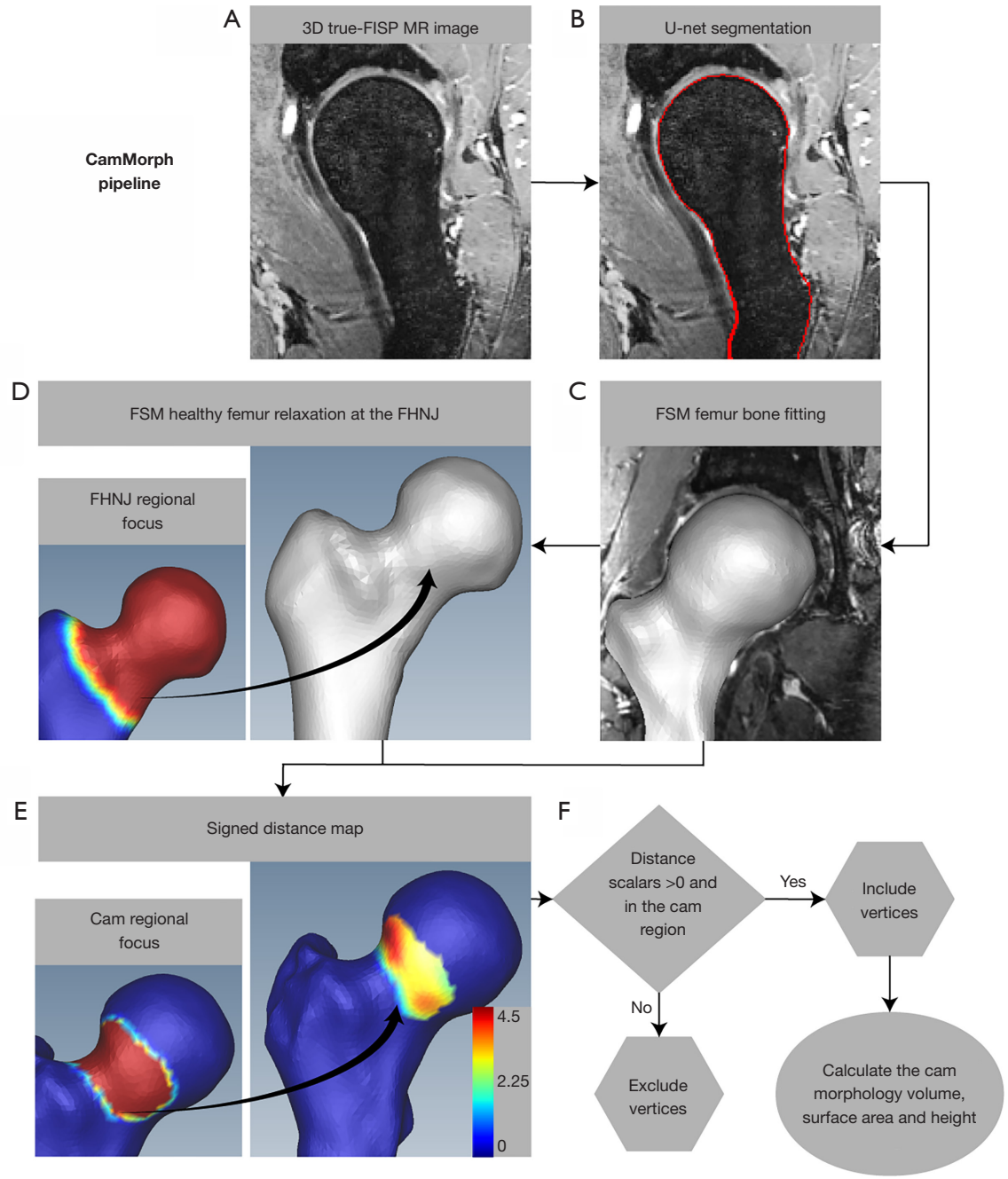

Figure 1 The CamMorph pipeline involving segmentation of the proximal femur and cam morphology as used in the analysis of MR images from the Australian FASHIoN study (Dataset C). (A) Initial 3D true-FISP MR image. (B) U-net femur bone segmentation. (C-F) Cam morphology segmentation for calculation of cam volume, surface area and height. 3D, three-dimensional; true-FISP, true fast imaging with steady-state precession; MR, magnetic resonance; FSM, focused shape model; FHNJ, femoral head-neck junction.

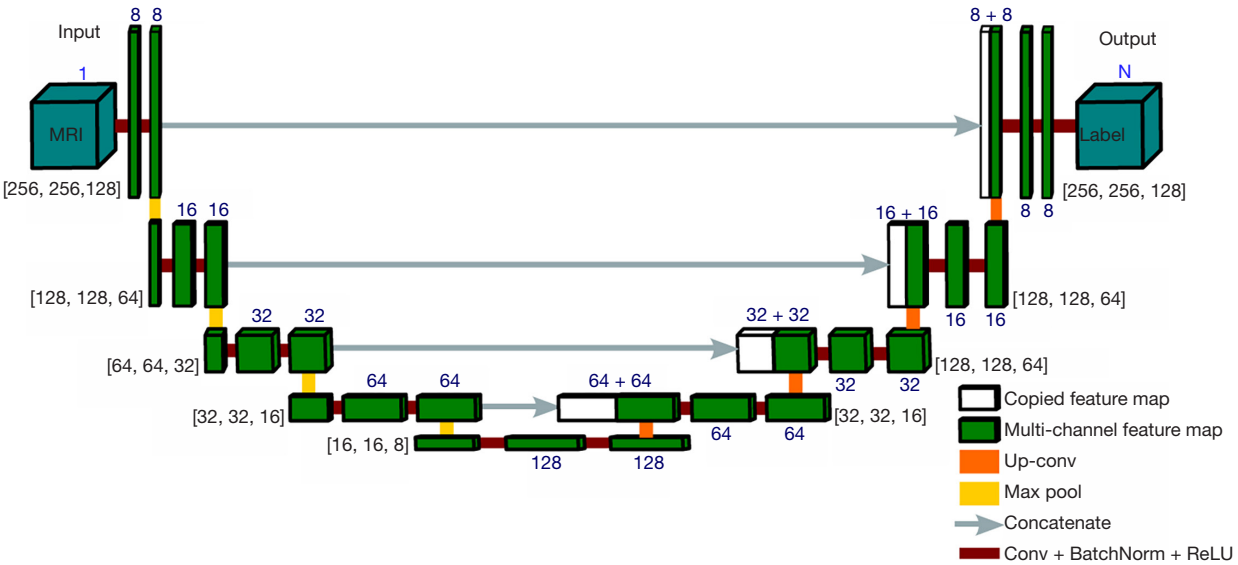

Figure 2 U-net architecture. Each green box corresponds to a multi-channel feature map. The number of channels is denoted above or below the box (in blue text). The X-Y-Z-size is provided at the lower left or right edge of the box (in black text). White boxes represent copied feature maps. The grey arrows denote concatenate operations, orange boxes correspond to up-convolution operations, yellow boxes denote max pool operations and brown boxes represent a multiple operations step of convolution, batch normalization and a rectified linear unit. MRI, magnetic resonance image; N, number of output label classes (i.e., background, femur, acetabulum); up-conv, up-convolution operation; max pool, max pool operation; concatenate, concatenate operation; conv, convolution operation; BatchNorm, batch normalization operation; ReLU, rectified linear unit.

femoral head-neck region (see the left image in *Figure 1D* where red indicates the ROI for femoral head-neck relaxation and blue is outside the ROI for relaxation). Here, 'relaxation' refers to the process by which the FSM reconstructs the cam-affected femur bone within the femoral head and neck region without any cam morphology knowledge. As a result, any existing cam morphology is relaxed to obtain a simulated 'healthy' femur bone (i.e., cam morphology is removed). After these steps, the position and size of the cam morphology is determined using the positive distance from the 3D simulated 'healthy' bone surface to the 3D cam-affected bone surface in the anterior and anterosuperior quadrant of the femoral head-neck region (*Figure 1E,1F*). The right image in *Figure 1E* displays a 3D femoral bone model with signed distance map scalars (units in mm) representative of the distance between the cam-affected and simulated 'healthy' bone surface. In *Figure 1E*, the distance scalars outside the cam region were thresholded to a value of 0.0 mm for visualization purposes. The left image in *Figure 1E* shows the cam region defined within this study (where red indicates the ROI and blue is outside this ROI). *Figure 1F* shows a flow chart indicating that only vertices with a positive distance from the simulated 'healthy' bone (in the cam region) were included in cam morphology calculations.

Initial automated 3D U-net based segmentation of the proximal femur

The MR images from Dataset A (12) were pre-processed with BSpline image resampling (0.5 mm isotropic), joint locator-based ROI extraction, denoising and N4 bias field correction. An isotropic resampling of 0.5 mm was chosen based on the high-resolution (0.23×0.23×0.46 mm^3) of the unilateral true-FISP images within Dataset A. Subsequently, the 3D U-net networks (see below) were trained on Dataset A for proximal femur volume segmentation.

3D U-net architecture

The network architecture used in the present work was based on a 3D U-net consisting of a down-sampling path and a symmetric up-sampling modified from its original form (16) for the hip joint (*Figure 2*). The down-sampling

path consists of 5 convolutional blocks, which increases the number of feature channels from 1 to 128. Each down-sampling block has two convolutional layers (kernel size of 3×3×3, stride of 1×1×1) and a Maxpooling layer (pool size of 2×2×2). The fifth block without the Maxpooling layer acts as a bridge to connect both paths. The up-sampling path consists of 4 convolutional blocks, each of which starts with a deconvolutional layer (kernel size of 3×3×3, stride of 2×2×2) and a concatenation with the feature maps corresponding to the down-sampling path. Two convolutional layers are used in each up-sampling block which halve the number of feature channels. All convolutional layers in both down-sampling and up-sampling paths use batch normalization, rectified linear unit activation and 'same' padding (to ensure the output image size is the same as the input image size). In the last layer of the up-sampling path, a 1×1×1 convolution with the Softmax activation function is used to map the multi-channel feature maps to the number of label classes N (N=3; background, femur, acetabulum).

Training and segmentation

All images with manual labels from Dataset A were pre-processed and cropped into an image size of 256×256×128. A 7-fold cross-validation procedure was used where the entire dataset was divided into 7 random subsets. In this procedure, 7 independent training iterations (with 3 repeats) were executed in parallel where each time a different subset of images was used for testing and the other 6 subsets of images for training. For each training iteration, 3D data augmentation (including affine transformation and elastic deformation) was applied to increase the diversity of the training data. Additionally, the Mixup technique was used to reduce the likelihood of overfitting and further improve the network performance (18). During the training process, we used the DSI as the loss function and the adaptive moment estimator (Adam) for parameter optimization (learning rate =0.0001). The entire training procedure resulted in an ensemble of 21 (7×3 repeats) 3D U-net networks for segmentation of the femur and acetabulum of the hip joint.

Segmentation and analysis of Dataset C

All the trained 3D U-net networks were used to automatically segment the bones of the hip joint from the clinical MR images in Dataset C (the FASHIoN dataset), which were independent from the MR data used in the U-net training phase (Dataset A) and FSM generation (Dataset B). Briefly, to segment a new hip MR image, trained 3D U-nets were used to generate a series of predictions for the femoral and acetabular bones from the pre-processed image. The final segmentation was obtained by averaging the multiple predicted labels and selecting the predicted label with a probability of more than 0.5. In the present study, only the femur was used in further processing. The subsequent application of the FSM, which simultaneously utilizes image features and priors (shape and appearance) with a distributed weighting identifying the most clinically important areas, improves the U-net segmentations within areas of interest, while conforming to anatomical constraints.

Cam segmentation and measurement pipeline

The following section describes the steps for FSM and atlas-based femur bone model initialization, the generation of a simulated 'healthy' bone model and the identification of cam morphology for calculating cam volume, surface area and height data from Dataset C.

FSM femur bone model initialization

Initially, a rough fitting of a 3D proximal femur bone model to the MR image was completed based on the centre of the femoral head (17), followed by FSM-based surface refinement (14) using the U-net segmentations (*Figure 1C*). The femoral head-neck ROI on the femur models was defined as shown by the red shading in *Figure 1D*. The DSI values of the U-net + FSM compared to manual segmentations were used to identify an atlas set to optimise the fitting performance of the U-net + FSM segmentation. For cases with DSI <0.95, the initial fitting models were improved using atlas-based registration with the atlas set consisting of cases with DSI ≥0.95 fitting accuracy.

Healthy femur bone generation

A simulated 'healthy' femur bone model was generated for each patient (*Figure 1D*) using a FSM (14) focusing on the femoral head-neck region (see left image in *Figure 1D*). This FSM was created using the training surfaces from Dataset B, as per Xia *et al.*'s work (13). A total of three eigenmodes accounting for 92% of shape variations were visually inspected using the simple medical imaging library interface (SMILI) (19) and used in an effort to exclude any

eigenmodes associated with cam morphology. This visual inspection consisted of a review of all shape variations within the first three eigenmodes within the anterior and anterosuperior femoral head-neck region. It was confirmed that these eigenmodes did not contain any cam morphology knowledge. Therefore, a FSM reconstruction of the cam-affected femur bone model within the femoral head and neck region simulated a 'healthy' femur bone (i.e., cam morphology is removed). This visual inspection was completed during the algorithm development of CamMorph prior to the initialization of the automated CamMorph pipeline. The CamMorph pipeline does not require this visual inspection when applied to an FAI dataset.

Constrained cam extent and location determination for cam morphology analysis

Distance-based methods with regional constraints were used to identify the location and quantify the size characteristics of cam morphology. A signed distance map was calculated between the reconstructed 'healthy' proximal femur and the cam-affected femur surface, using the Visualization Toolkit (VTK) (20) (*Figure 1E*). The distance map scalars were overlayed onto the femoral surface using SMILI (19).

The anterior and anterosuperior femoral head-neck region (typical location of cam formations) was manually contoured onto the femoral surface (see left image in *Figure 1E*) using SMILI (19) prior to the initialization of the automatic CamMorph pipeline. All cases utilized the same contour within the presented workflow. If a vertex on the femoral model was identified to be within this contoured region and the respective femur surface vertex on the distance model had a value of more than 0, the vertex was included as part of a cam morphology formation (*Figure 1F*). The cam volume and surface area were calculated using VTK (20) and SMILI (19). The cam height data was obtained at each vertex on the femoral surface using the previously calculated distance map [using a signed distance map from VTK (20)], between the simulated 'healthy' femur bone surface and the cam-affected femur surface within the cam ROI. The cam maximum- and average-height were calculated from the set of cam height values obtained for each patient. The cam volume, surface area, maximum- and average-height were used for the primary data comparison between male and female FAI patients in the present study.

Femoral head volume analyses

In a secondary data analysis, values for femoral head volume (see below) were compared between the male and female FAI patients (Dataset C) to assess previously reported sexual dimorphism for this anatomical measure (21-23) and to determine cam volume as a percentage of femoral head volume. The calculation of femoral head volume involved initial resampling of the MR images to be isotropic. Estimations of the femoral head centre and radius were obtained in 3D using the circle Hough transform as per Nishii *et al.* (17). Subsequently, a refined segmentation of the femoral head used the U-net segmentation to only include voxels within both the U-net and circle Hough transform-based segmentation. This refined segmentation was required to define the boundary between the femoral head and neck within the U-net segmentation for subsequent femoral head volume calculation.

Statistical analyses

For both the primary data (cam volume, surface area, maximum- and average-height) and secondary data analyses (femoral head volume, cam volume: femoral head volume percentage), independent *t*-tests or Mann-Whitney U rank tests were used for comparisons between the male and female FAI patients. The Shapiro-Wilk test was performed to check the normality of the data and Mann-Whitney U rank tests were used if the data did not have a normal distribution. The Levene test was used to check for homogeneity of variances and Welch's procedure was applied when the sample variances were not equal. The Pearson correlation coefficient was used to assess the association between cam volume and other cam metrics (surface area, maximum- and average-height) in the male and female patients. Statistical significance was accepted at $P<0.05$ and analyses were performed using a python package, SciPy (24).

Results

Manual and automated proximal femur segmentation

Figure 3 shows boxplots for the DSI (*Figure 3A*), 95% HD (*Figure 3B*) and ASD values (*Figure 3C*) for the manual and automated bone segmentations of the proximal femur volume obtained from Dataset C. Overall, the 3D U-net + FSM approach (as implemented in the CamMorph pipeline)

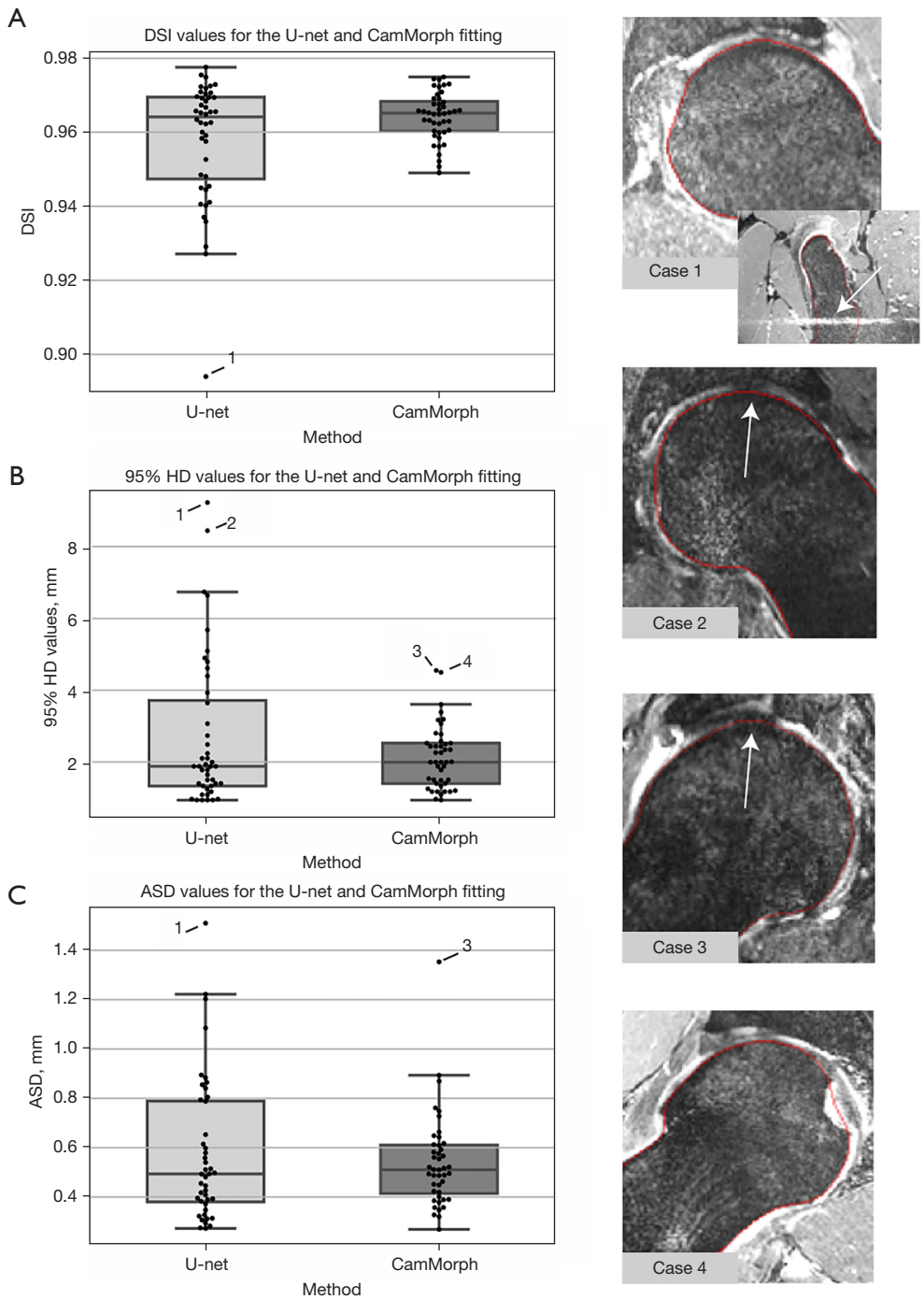

Figure 3 Boxplots of the evaluation metrics used in this study for the manual and automated segmentations of the proximal femur [U-net alone and U-net + FSM (CamMorph)]. (A) DSI values. (B) 95% HD values. (C) ASD values. The boxplot centreline marks the median value. The inset coronal magnetic resonance images show the relatively poorer image quality for outlier cases with the automated segmentation contour overlayed. Case 1 shows nonconforming image contrast characteristics, both Cases 1 and 2 have motion/image artefacts (Case 1 white arrow in sagittal image indicates artefacts), Cases 2 and 3 show comparatively poor bone cartilage interface contrast (white arrows) and Case 4 has, like all the outlier cases shown, incomplete coverage of the femoral neck-greater trochanter region, and a prominent foveal region with surrounding bright synovial fluid which caused difficulty during the FSM fitting. DSI, Dice similarity index; HD, Hausdorff distance; ASD, average surface distance; FSM, focused shape model.

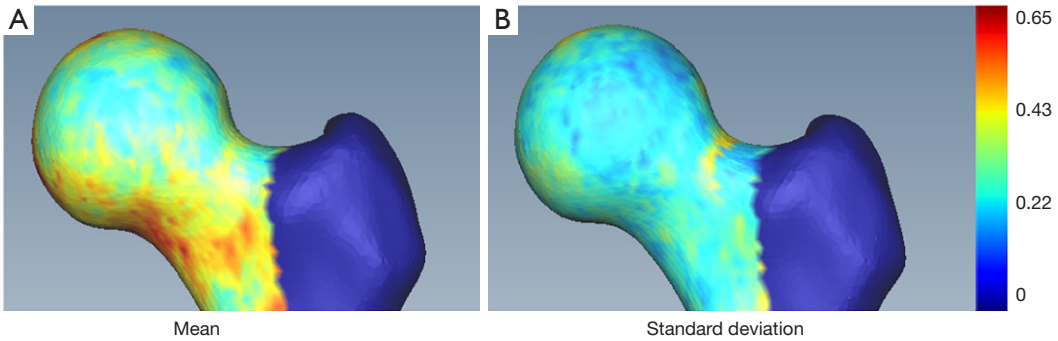

Figure 4 The 95% HD between the U-net + FSM and the manual segmentations of the proximal femur. (A) Mean 95% HD. (B) Standard deviation 95% HD. The HD scalar bar (rainbow colour map on right side of the figure) has units in mm. The greater trochanter region and femur shaft region were given a value of zero for visualization purposes. HD, Hausdorff distance; FSM, focused shape model.

had an enhanced performance compared to the U-net alone having better mean scores and decreased spread for the DSI (U-net =0.958±0.017; U-net + FSM =0.964±0.006), 95% HD (U-net =2.717±2.089 mm; U-net + FSM =2.123± 0.876 mm) and ASD (U-net =0.577±0.289 mm; U-net + FSM =0.539±0.189 mm) values.

Each proximal femur model from the 3D U-net + FSM segmentation was analysed separately using the 95% HD value. The mean and standard deviation HD between the U-net + FSM and manual segmentations are shown in *Figure 4A*,*4B*, respectively. Overall, the U-net + FSM result within the femoral head-neck region of the femur, of primary interest in the current study, was in very strong agreement with the manual segmentation. Notably, the weighted average image spacing within this study was 0.644×0.644×0.668 mm, where on average the highest surface distance accuracy attainable within this study is 0.644 mm (the smallest average image spacing dimension). Observations from *Figure 4A*,*4B* indicate that the 95% HD values within the femoral head-neck region were below 0.65 mm in both the mean and standard deviation visualizations, respectively. These results indicate the high surface-based accuracy of the CamMorph pipeline which was robust to the spectrum of pathology and image-based issues within Dataset C. In the current study, the greater trochanter and the included shaft region of the femur had larger HD values, however these are not clinically important areas for cam morphology assessment.

Cam volume, surface area and height

Figure 5 displays boxplots, and *Table 1* provides a summary of the mean and standard deviation data, for the cam volume, surface area, maximum- and average-height measurements for the male and female patients from Dataset C. Compared to females, males had a significantly larger median cam volume (969.22 *vs.* 272.97 mm^3, P<0.001), mean surface area (657.36 *vs.* 306.93 mm^2, P<0.001) median maximum-height (3.66 *vs.* 2.15 mm, P<0.001) and median average-height (1.70 *vs.* 0.86 mm, P<0.001). In the male and female FAI patients, cam volume was classified based on quartile data (*Table 2*), as negligible (≤Q1), mild (>Q1 and ≤Q2), moderate (>Q2 and ≤Q3), or major (>Q3).

For the male and female FAI patients, there were strong postitive correlations betweeen cam volume and surface area (*Figure 6A*,*6B*), cam volume and maximum-height (*Figure 6C*,*6D*) and cam volume and average-height (*Figure 6E*,*6F*).

Figure 7 shows 3D models of the proximal femur which were generated in SMILI (19) to show the cam profiles in individual female and male patients classified as having a negligible (*Figure 7A*,*7E*), mild (*Figure 7B*,*7F*), moderate (*Figure 7C*,*7G*) or major (*Figure 7D*,*7H*) cam volume. Inspection of the cam profiles allows for comparative visual analysis within and between the classification categories; for example, *Figure 7C* shows the cam profile in a female patient classified with a moderate cam volume where the cam surface area profile is smaller than that in a female patient classified with a mild cam volume (*Figure 7B*).

Femoral head volume

Figure 8 displays boxplots of the femoral head volumes for the male and female FAI patients from Dataset C. Compared to female patients, male patients had a

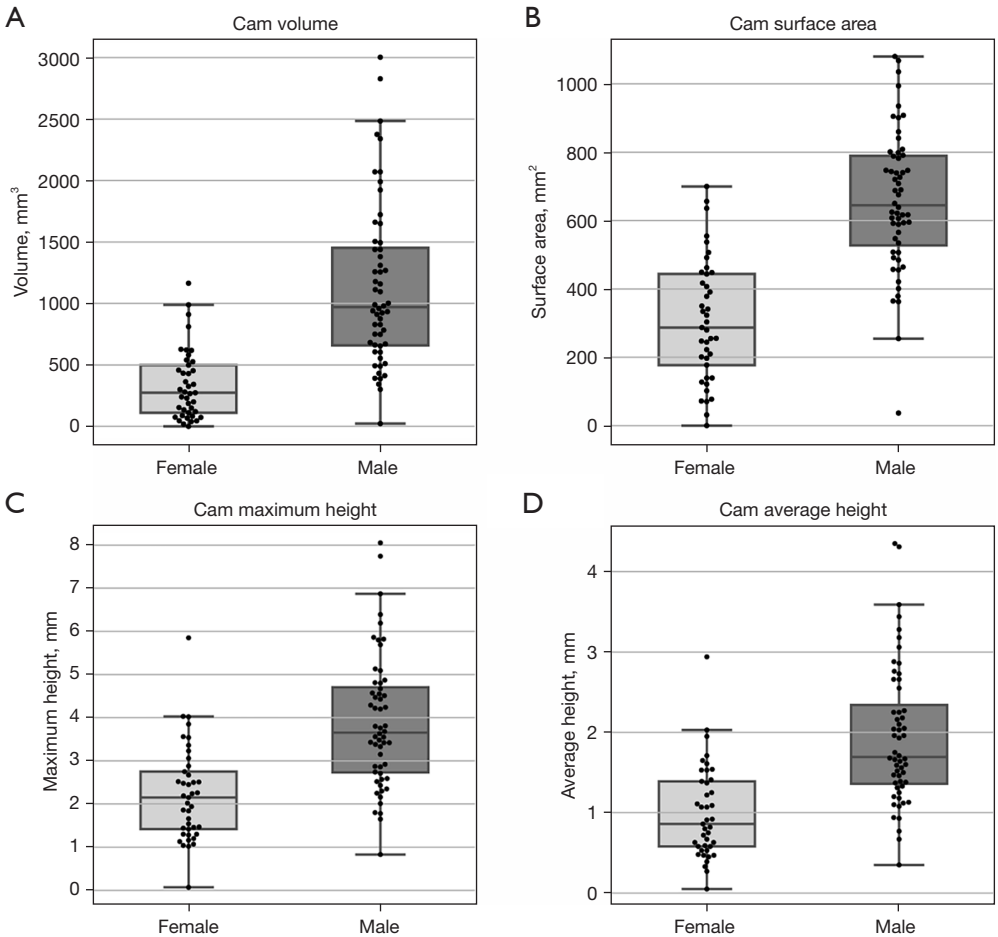

Figure 5 Boxplots of cam size metrics for female and male patients. (A) Cam volume. (B) Cam surface area. (C) Cam maximum-height. (D) Cam average-height (D). The boxplot centreline marks the median value.

Table 1 Mean and standard deviation data for cam volume, surface area, maximum- and average-height in the male and female FAI patients

Measurements	Male patients	Female patients	P value
Volume (mm^3)	1,136.87±659.83	337.86±279.95	<0.001
Surface area (mm^2)	657.36±203.04	306.93±175.61	<0.001
Maximum-height (mm)	3.89±1.51	2.23±1.09	<0.001
Average-height (mm)	1.94±0.86	1.00±0.57	<0.001

FAI, femoroacetabular impingement.

Table 2 Cam volume quartiles used for classifying cam volume in the male and female FAI patients

Quartile	Male patients	Female patients
Q1	657.38 mm^3	111.06 mm^3
Q2	969.22 mm^3	272.97 mm^3
Q3	1,466.51 mm^3	497.93 mm^3

FAI, femoroacetabular impingement.

significantly larger mean femoral head volume [66.12 *vs.* 46.02 cm^3, t(95)=13.21, P<0.001]. *Figure 9* shows boxplots of the cam volume to femoral head volume, in percentage terms, for the male and female FAI patients. The median cam volume to femoral head volume percentage for the male patients was significantly larger than the female patients (1.47 *vs.* 0.59, U=389.0, P<0.001).

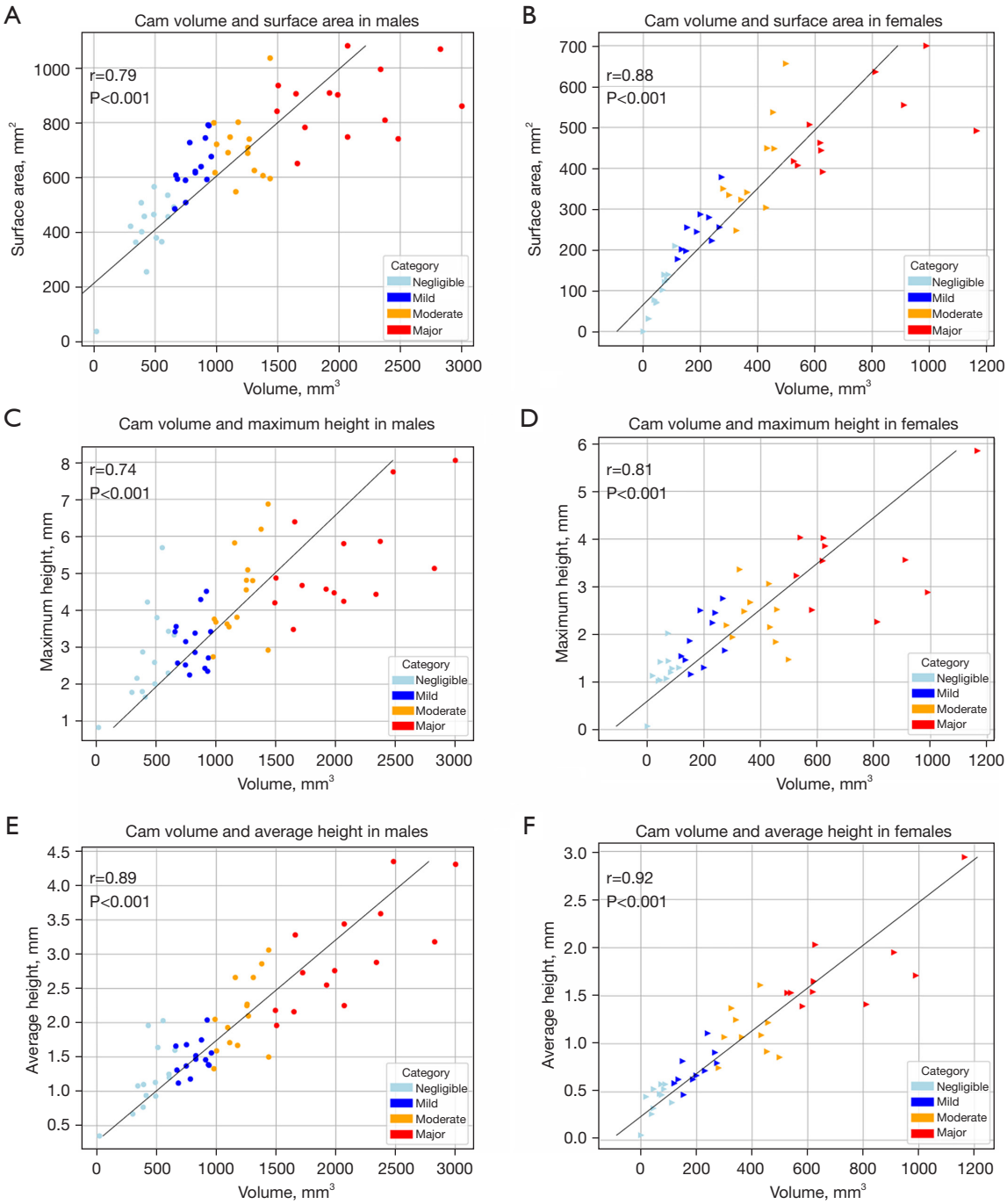

Figure 6 Scatterplots and regression line analysis of cam size metrics for male and female patients. (A,B) Cam volume *vs.* surface area. (C,D) Cam volume *vs.* maximum-height. (E,F) Cam volume *vs.* average-height. The left column displays male results, and the right column displays female results.

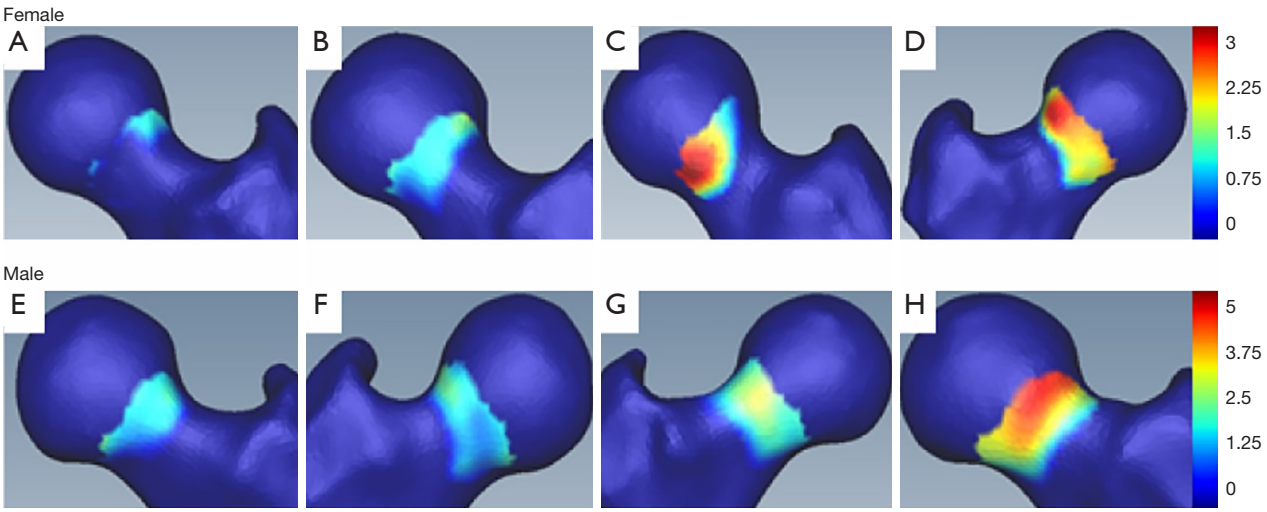

Figure 7 3D proximal femoral bone models for visualization of cam profiles in individual female and male patients with different cam volume classifications. (A,E) Negligible cam volumes. (B,F) Mild cam volumes. (C,G) Moderate cam volumes. (D,H) Major cam volumes. The top row displays female results, and the bottom row displays male results. A separate scalar bar (rainbow colour map) for females and males provides cam height in mm. 3D, three-dimensional.

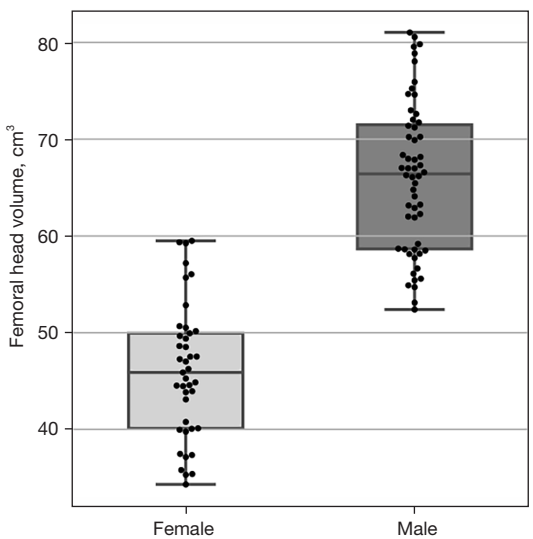

Figure 8 Boxplots of femoral head volumes in female and male patients. The boxplot centreline marks the median value.

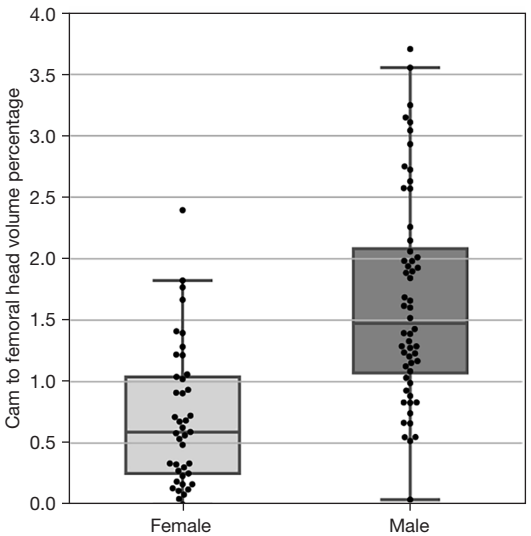

Figure 9 Boxplots of the cam volume to femoral head volume percentage in female and male patients. The boxplot centreline marks the median value.

Discussion

The present study involved the successful development of a novel, fully automated 3D cam morphology extraction pipeline which provided patient-specific, direct measures of cam volume, surface area and height from multi-site clinical MR images in male and female patients with FAI. The data calculated from the CamMorph pipeline showed there was significantly greater cam volume, surface area, maximum- and average-height in male, compared to female, FAI patients. In conjunction with the quantitative analyses of cam morphology provided by the CamMorph pipeline, 3D bone models of the proximal femur were generated from the automated segmentations of the MR images from

individual patients allowing visualization of differences in cam morphology within and between male and female FAI patients classified with a negligible, mild, moderate or major cam volume. Overall, the developed CamMorph pipeline combined the substantial abilities of the 3D U-net to localize both global (region) and local (edge) features in MR images and a FSM to generate an anatomical model for creating patient-specific models of the proximal femur to provide a robust automated approach for extracting cam morphology and measuring cam volume, surface area and height from clinical 3D MR images in patients with differing FAI severity and pathoanatomical characteristics. The calculation of cam volume, surface area and height data by the fully automated CamMorph pipeline was achieved in under 5 min which is well suited for potential application in clinical environments.

Proximal femur segmentation

The high degree of agreement between the manual and automated CamMorph segmentations of proximal femur volume (mean DSI of 0.964) in the present work compares very favourably with previous studies on automated segmentation of the femur from MR images (25-29) [see Table S1 for specific data (14,26,30-36)]. Overall, the combined 3D U-net + FSM approach used in the CamMorph pipeline resulted in a decreased spread of the DSI values (along with an overall increase in the mean value) compared with the U-net alone segmentations of the proximal femur volume. Enhanced performance of the CamMorph pipeline compared with the U-net alone approach was similarly found for the 95% HD and ASD data highlighting the increased efficacy of the combined U-net + FSM approach for the segmentation of the proximal femur in the clinical MR images obtained from FAI patients in the Australian FASHIoN study. Notably, the high surface-based accuracy for segmentation of the proximal femur in the clinical MR images by the automated CamMorph pipeline was achieved in the presence of variable motion artefacts, contrast differences and FOV issues (insufficiencies) within the multi-site FASHIoN dataset. For the femoral head-neck region specifically, the majority of the mean 95% HD values between the manual and automated CamMorph segmentations were between 0 to 0.65 mm highlighting the robustness of the combined U-net + FSM approach for targeted segmentation of bone in this clinical ROI in the MR images of the male and female FAI patients.

Cam volume, surface area and height

The automated CamMorph pipeline presented in the current paper successfully integrated patient-specific healthy models derived from individualised cam-affected models of the proximal femur for the calculation of cam volume, surface area and height data. Previously, Kang *et al.* (10) proposed calculation of cam morphology with reference to healthy bone models although they used an average model derived from 4 separate femur models from asymptomatic subjects obtained through manual segmentation whereas we used patient-specific healthy models derived from the automated analyses of FAI patients' 3D MR images. The use of the automated 3D CamMorph pipeline to measure cam morphology, as opposed to manual (10) and semi-automated (9,23,37-40) approaches, offers a fast (under 5 min), robust method which can be run in the background post-MR acquisition to obtain patient-specific data well suited for routine clinical examinations, as well as for larger-scale clinical trials such as the Australian FASHIoN study.

In the present analysis of the FASHIoN MR dataset, the median cam volume in male patients (0.97 cm^3) was significantly greater than in the female patients (0.27 cm^3). Recently, Guidetti *et al.* performed arthroscopic removal of cam bone mass from the hemipelvis of 7 cadavers (sex not specified) and reported that the surgically excised cam volumes, as determined from semi-automated MR measurements, ranged between 0.25 to 1.75 cm^3 (41) which is in good general agreement with our range of cam volumes determined in the male (0 to 3.0 cm^3) and female patients (0 to 1.16 cm^3) using the CamMorph pipeline (Table S2).

Previous CT studies (9,23,37) have reported larger mean cam volumes (e.g., 4.3 cm^3 in females, 6.7 cm^3 in males, 4.6 to 7.96 cm^3 in mixed sex cohorts) from segmentations using a semi-automated region-growing technique based on density values without any reference to the 3D shape profile of the femoral head-neck region. Whilst the substantial differences between the MR derived [current study, Guidetti *et al.* (41)] and CT derived cam volumes (9,23,37) may be due to real differences in the severity of the cam lesions in these study cohorts, it may relate to an over-estimation of cam volume in the CT studies due to the region-growing approach systematically over-segmenting areas within the lower bone density supero-lateral quadrant of the femoral head (42). An over-segmentation of cam volume in the above CT studies could account for scenarios such as the relative volume of a cam bone mass (11.1 cm^3) being 29% of that compared to femoral head volume (39.1 cm^3)

as reported by Schauwecker *et al.* (37). In the most extreme cases in the present MR study, the relative cam to femoral head volume was below 4% for the male and female patients with FAI (*Figure 9* and Figure S1).

The greater cam volume in males compared to females observed in the present study is consistent with the overall findings from previous CT studies (23,40). Currently, understanding of this sex-based difference in cam volume is incomplete but it may be associated with factors such as males generally having greater absolute body size, higher magnitude loading of the hip joint or specific sex-related dimorphism in the anatomical and alignment characteristics of the femur and acetabulum. Studies have also reported that cam morphology is typically more prevalent in males with FAI whereas pincer morphology of the acetabulum is observed relatively more in female patients although the presence of both cam and pincer morphology, the so called mixed-type FAI, is also common in both male and female patients (43). In the Australian FASHIoN study, patients were included on the basis of hip pain and plain radiographs considered to show signs of FAI related to either cam morphology (e.g., alpha angles >55°), pincer morphology (e.g., lateral centre edge angle >40°, positive cross-over sign) and/or mixed-type FAI rather than being solely restricted to those with cam morphology only; this assortment of presentations is consistent with the automated CamMorph measures of cam volumes ranging from negligible to major determined from the baseline MR images of the male and female FAI patients in the present analyses.

Compared to female FAI patients, male patients had a significantly larger mean cam surface area (6.57 *vs.* 3.07 cm^2), median maximum-height (3.66 *vs.* 2.15 mm) and median average-height (1.70 *vs.* 0.86 mm) based on the automated CamMorph analysis of the FASHIoN MR dataset. These values agree well with the mean cam surface area (6.158 cm^2), maximum-height (3.7 mm) and average-height (1.6 mm) reported from MR measures obtained in the cadaver study of Guidetti *et al.* (41). Kang *et al.* reported, based on MR measurements, a considerably smaller mean cam surface area (0.52 cm^2), which may be related to a suboptimal fitting of the average 'healthy' model to the pathological femur bone models (10). Moreover, their mean cam average-height (3.9 mm) was notably different to the median values obtained from the MR measures in our current work and mean values from Guidetti *et al.*'s study (41). The use of average 'healthy' models by Kang *et al.* (10), rather than an individual patient model as per the developed CamMorph approach, may account for these differing outcome data.

Strong positive correlations were observed between cam volume and surface area, cam volume and maximum-height and cam volume and average-height in the male and female patients from the FASHIoN study (*Figure 6*). There were, however, notable cam profile differences visualized in the 3D bone models of the proximal femur in individual patients classified as having negligible, mild, moderate or major cam volumes (*Figure 7*). These differences suggest that cam morphology may present with a spectrum of topological forms in FAI patients although further systematic shape-based analyses are required to explore this aspect across factors such as sex, anthropometry and FAI severity.

Femoral head volume

In the present study, analysis of the mean femoral head volume showed male patients (66.12 cm^3) had significantly greater volumes than the female patients (46.02 cm^3). The femoral head volumes derived from our automated segmentation approach are consistent with values reported in earlier CT and MRI studies (9,21-23,37,40) (Table S3) and studies reporting significantly greater femoral head volumes (21-23) and radii (40) in males compared to females. In previous MR arthrography (21), CT (9,23,37) and cadaveric studies (22), femoral head volume has been calculated using manual segmentation (21), region growing methods (based on CT density) (9,23,37) and direct anatomical measurements using callipers (22), whereas there was no manual (or semi-automated) processing required in the current analyses of the MR images in the FAI patients. Furthermore, our automated segmentation of femoral head volume was robust to varying MR image contrast characteristics and artefacts, differing imaging FOV and the presence of osteophytes and increased synovial fluid surrounding the bone-cartilage interface of the femoral head.

There was a significantly greater median cam volume to femoral head volume percentage in male compared to female FAI patients (1.5% *vs.* 0.6%). A higher median percentage cam volume to femoral head volume in male FAI patients was also established from data obtained from male (10.4%) and female (9.2%) patients in a previous CT study (23). The higher percentage values calculated in the Zhang *et al.* study (23) were associated with substantially larger cam volumes compared to our values which may reflect an overall greater severity of cam mass in their FAI patients or

alternatively, be related to the use of regional bone density values for determining cam morphology. Further studies on male and female FAI patients are required to better clarify the association between cam volume and femoral head volume stratified by sex.

In the present study, the automated CamMorph pipeline was successfully developed (Datasets A and B) and implemented (Dataset C) using 3D true-FISP and DESS MR images from three separate databases. Future work assessing the ability of CamMorph to segment and analyze cam morphology from other 3D MRI sequences such as the volumetric interpolated breath hold examination (VIBE) and the sampling perfection with application optimized contrasts using different flip angle evolution (SPACE) sequence, which, along with 3D true-FISP, have been shown to provide bone volumes comparable to CT in a cadaveric study of the knee (44), would be beneficial for further evaluation of our U-net + FSM approach for analysing bone formations in symptomatic conditions such as FAI. Comparisons between MR and CT-based cam measures obtained with CamMorph could be conducted to assess the respective data obtained from these two modalities notwithstanding the clinical advantages of MRI for simultaneous evaluation of bony, cartilaginous and associated soft tissues of the hip joint without exposing patients to ionizing radiation.

The cam volume, surface area and height measurements in our study were in good agreement with corresponding data reported in Guidetti *et al.*'s study based on MR analysis of arthroscopically excised cam bone mass from cadavers (41). In future MR (or CT) studies, the cam morphology measures obtained with CamMorph could be compared directly with "ground truth" data from arthroscopic cam excision although precise delineation of cam bone mass in both pre-operative (cam bone mass identified for removal) and post-operative (actual cam bone mass removed) analyses would be essential for the validity of any investigations.

In conjunction with cam morphology measures, the developed 3D CamMorph pipeline offers the potential for future research involving comprehensive shape-based analyses of cam location and topology in MR images of the hip joint acquired from a range of individuals (e.g., asymptomatic/symptomatic, athlete/non-athlete, surgically/non-surgically managed cohorts). Clinically, shape based analyses could be used for detailed assessment of cam characteristics in cross-sectional (e.g., patients with non-dysplastic *vs.* dysplastic hips) or longitudinal studies (e.g., patients treated conservatively *vs.* surgically). In FAI patients, these analyses could be used to help inform clinical assessments in regards to patient symptoms, pre- and post-intervention treatment evaluations and patient reported outcome data such as that collected in the current FASHIoN trial. Shape analyses may also offer insights into cam bone morphology in relation to anthropometric characteristics or history of sporting (physical) activity levels.

Further improvements to the 3D CamMorph pipeline could include an automated assessment of acetabular pincer-related morphology. This would involve generating a separate acetabulum FSM using data from individuals without pincer morphology. Subsequently, the central steps in the present work involving 3D U-net + FSM segmentation and simulated 'healthy' bone creation would be followed. In terms of clinical application, cam and pincer morphology data could be used for both pre- and post-arthroscopic analysis. The 3D proximal femur models generated from CamMorph could also be utilized to improve patient education.

Conclusions

The fully automated 3D CamMorph pipeline developed in the present study successfully segmented and measured cam morphology from clinical MR images of the hip in male and female patients with differing FAI severity and pathoanatomical characteristics.

Acknowledgments

We would like to thank Professor Kim Bennell who was a Principal Investigator for the FASHIoN trial and was involved in the data collection for the MR images used in this study.

Funding: This work was supported by the University of Queensland and the Australian e-Health Research Centre under the Multi-Institutional Agreement for the National Health and Medical Research Council Development Grant APP1139868 entitled "MR Hip Intervention and Planning System to Enhance Clinical and Surgical Outcomes".

Footnote

Reporting Checklist: The authors have completed the MDAR reporting checklist. Available at https://qims.amegroups.com/article/view/10.21037/qims-22-332/rc

Conflicts of Interest: All authors have completed the ICMJE uniform disclosure form (available at https://qims.amegroups.com/article/view/10.21037/qims-22-332/coif). SSC, SC, JF and CE report grants from the National Health and Medical Research Council during the conduct of the study. DJH reports personal fees from Pfizer, Lilly, TLCBio, Novartis, Tissuegene, Biobone outside the submitted work. The other authors have no conflicts of interest to declare.

Ethical Statement: The authors are accountable for all aspects of the work in ensuring that questions related to the accuracy or integrity of any part of the work are appropriately investigated and resolved. The study was conducted in accordance with the Declaration of Helsinki (as revised in 2013).

References

1. Frasson VB, Vaz MA, Morales AB, Torresan A, Telöken MA, Gusmão PDF, Crestani MV, Baroni BM. Hip muscle weakness and reduced joint range of motion in patients with femoroacetabular impingement syndrome: a case-control study. Braz J Phys Ther 2020;24:39-45.
2. Fernquest S, Palmer A, Gimpel M, Birchall R, Broomfield J, Wedatilake T, Dijkstra H, Burchall J, Lloyd T, Pereira C, Newman S, Carr A, Glyn-Jones S. A longitudinal cohort study of adolescent elite footballers and controls investigating the development of cam morphology. Sci Rep 2021;11:18567.
3. Harris MD, Kapron AL, Peters CL, Anderson AE. Correlations between the alpha angle and femoral head asphericity: Implications and recommendations for the diagnosis of cam femoroacetabular impingement. Eur J Radiol 2014;83:788-96.
4. van Klij P, Reiman MP, Waarsing JH, Reijman M, Bramer WM, Verhaar JAN, Agricola R. Classifying Cam Morphology by the Alpha Angle: A Systematic Review on Threshold Values. Orthop J Sports Med 2020;8:2325967120938312.
5. Sutter R, Dietrich TJ, Zingg PO, Pfirrmann CW. How useful is the alpha angle for discriminating between symptomatic patients with cam-type femoroacetabular impingement and asymptomatic volunteers? Radiology 2012;264:514-21.
6. Agricola R, Waarsing JH, Thomas GE, Carr AJ, Reijman M, Bierma-Zeinstra SM, Glyn-Jones S, Weinans H, Arden NK. Cam impingement: defining the presence of a cam deformity by the alpha angle: data from the CHECK cohort and Chingford cohort. Osteoarthritis Cartilage 2014;22:218-25.
7. Barrientos C, Barahona M, Diaz J, Brañes J, Chaparro F, Hinzpeter J. Is there a pathological alpha angle for hip impingement? A diagnostic test study. J Hip Preserv Surg 2016;3:223-8.
8. Cohen D, Khan A, Kay J, Slawaska-Eng D, Almasri M, Simunovic N, Duong A, Safran MR, Ayeni OR. There is no definite consensus on the adequate radiographic correction in arthroscopic osteochondroplasty for femoroacetabular impingement: a systematic review and meta-analysis. Knee Surg Sports Traumatol Arthrosc 2021;29:2799-818.
9. Dessouky R, Chhabra A, Zhang L, Gleason A, Chopra R, Chatzinoff Y, Fey NP, Xi Y, Wells J. Cam-type femoroacetabular impingement-correlations between alpha angle versus volumetric measurements and surgical findings. Eur Radiol 2019;29:3431-40.
10. Kang X, Zhang H, Garbuz D, Wilson DR, Hodgson AJ. Preliminary evaluation of an MRI-based technique for displaying and quantifying bony deformities in cam-type femoroacetabular impingement. Int J Comput Assist Radiol Surg 2013;8:967-75.
11. Murphy NJ, Eyles J, Bennell KL, Bohensky M, Burns A, Callaghan FM, et al. Protocol for a multi-centre randomised controlled trial comparing arthroscopic hip surgery to physiotherapy-led care for femoroacetabular impingement (FAI): the Australian FASHIoN trial. BMC Musculoskelet Disord 2017;18:406.
12. Xia Y, Chandra SS, Engstrom C, Strudwick MW, Crozier S, Fripp J. Automatic hip cartilage segmentation from 3D MR images using arc-weighted graph searching. Phys Med Biol 2014;59:7245-66.
13. Xia Y, Fripp J, Chandra SS, Schwarz R, Engstrom C, Crozier S. Automated bone segmentation from large field of view 3D MR images of the hip joint. Phys Med Biol 2013;58:7375-90.

14. Chandra SS, Xia Y, Engstrom C, Crozier S, Schwarz R, Fripp J. Focused shape models for hip joint segmentation in 3D magnetic resonance images. Med Image Anal 2014;18:567-78.
15. Litjens G, Toth R, van de Ven W, Hoeks C, Kerkstra S, van Ginneken B, et al. Evaluation of prostate segmentation algorithms for MRI: the PROMISE12 challenge. Med Image Anal 2014;18:359-73.
16. Çiçek Ö, Abdulkadir A, Lienkamp SS, Brox T, Ronneberger O. 3D U-Net: learning dense volumetric segmentation from sparse annotation. In: International conference on medical image computing and computer-assisted intervention. Cham: Springer, 2016:424-32.
17. Nishii T, Sugano N, Sato Y, Tanaka H, Miki H, Yoshikawa H. Three-dimensional distribution of acetabular cartilage thickness in patients with hip dysplasia: a fully automated computational analysis of MR imaging. Osteoarthritis Cartilage 2004;12:650-7.
18. Zhang H, Cisse M, Dauphin YN, Lopez-Paz D. mixup: Beyond empirical risk minimization. arXiv 2017:1710.09412.
19. Chandra SS, Dowling JA, Engstrom C, Xia Y, Paproki A, Neubert A, Rivest-Hénault D, Salvado O, Crozier S, Fripp J. A lightweight rapid application development framework for biomedical image analysis. Comput Methods Programs Biomed 2018;164:193-205.
20. Schroeder W, Martin K, Lorensen B. The visualization toolkit, 4th ed. New York: Kitware Inc., 2006.
21. Frank JM, Lee S, McCormick FM, Jordan M, Austell B, Slikker W, Salata MJ, Nho SJ. Quantification and correlation of hip capsular volume to demographic and radiographic predictors. Knee Surg Sports Traumatol Arthrosc 2016;24:2009-15.
22. Weinberg DS, Williamson DF, Millis MB, Liu RW. Decreased and increased relative acetabular volume predict the development of osteoarthritis of the hip: an osteological review of 1090 hips. Bone Joint J 2017;99-B:432-9.
23. Zhang L, Wells JE, Dessouky R, Gleason A, Chopra R, Chatzinoff Y, Fey NP, Xi Y, Chhabra A. 3D CT segmentation of CAM type femoroacetabular impingement-reliability and relationship of CAM lesion with anthropomorphic features. Br J Radiol 2018;91:20180371.
24. Virtanen P, Gommers R, Oliphant TE, Haberland M, Reddy T, Cournapeau D, et al. SciPy 1.0: fundamental algorithms for scientific computing in Python. Nat Methods 2020;17:261-72. Erratum in: Nat Methods 2020;17:352.
25. Zeng G, Wang Q, Lerch T, Schmaranzer F, Tannast M, Siebenrock K, Zheng G. Latent3DU-net: Multi-level latent shape space constrained 3D U-net for automatic segmentation of the proximal femur from radial MRI of the hip. In: International Workshop on Machine Learning in Medical Imaging. Cham: Springer, 2018:188-96.
26. Zeng G, Zheng G. Deep Learning-Based Automatic Segmentation of the Proximal Femur from MR Images. Adv Exp Med Biol 2018;1093:73-9.
27. Peng B, Guo Z, Zhu X, Ikeda S, Tsunoda S. Semantic segmentation of femur bone from MRI images of patients with hematologic malignancies. In: 2020 IEEE Region 10 Conference (Tencon), 2020:1090-4.
28. Memi A, Varlı S, Bilgili F. Semantic segmentation of the multiform proximal femur and femoral head bones with the deep convolutional neural networks in low quality MRI sections acquired in different MRI protocols. Comput Med Imaging Graph 2020;81:101715.
29. Deniz CM, Xiang S, Hallyburton RS, Welbeck A, Babb JS, Honig S, Cho K, Chang G. Segmentation of the Proximal Femur from MR Images using Deep Convolutional Neural Networks. Sci Rep 2018;8:16485.
30. Zeng G, Yang X, Li J, Yu L, Heng PA, Zheng G. 3D U-net with multi-level deep supervision: fully automatic segmentation of proximal femur in 3D MR images. In: International workshop on machine learning in medical imaging. Cham: Springer, 2017:274-82.
31. Zeng G, Zheng G. 3D tiled convolution for effective segmentation of volumetric medical images. In: International Conference on Medical Image Computing and Computer-Assisted Intervention. Cham: Springer, 2019:146-54.
32. Zeng G, Zheng G. Holistic decomposition convolution for effective semantic segmentation of medical volume images. Med Image Anal 2019;57:149-64.
33. Damopoulos D, Lerch TD, Schmaranzer F, Tannast M, Chênes C, Zheng G, Schmid J. Segmentation of the proximal femur in radial MR scans using a random forest classifier and deformable model registration. Int J Comput Assist Radiol Surg 2019;14:545-61.
34. Arezoomand S, Lee WS, Rakhra KS, Beaulé PE. A 3D active model framework for segmentation of proximal femur in MR images. Int J Comput Assist Radiol Surg 2015;10:55-66.
35. Zeng G, Zheng G. Deep volumetric shape learning for semantic segmentation of the hip joint from 3D MR images. In: International Workshop on Computational

Methods and Clinical Applications in Musculoskeletal Imaging. Cham: Springer, 2018:35-48.
36. Pham DD, Dovletov G, Warwas S, Landgraeber S, Jäger M, Pauli J. Deep segmentation refinement with result-dependent learning. In: Handels H, Deserno TM, Maier A, Maier-Hein KH, Palm C, Tolxdorff T. editors. Bildverarbeitung für die Medizin 2019. Wiesbaden: Springer Vieweg, 2019:49-54.
37. Schauwecker N, Xi Y, Slepicka C, Dessouky R, Fey N, Chatzinoff Y, Chopra R, Wells J, Chhabra A. Quantifying differences in femoral head and neck asphericity in CAM type femoroacetabular impingement and hip dysplasia versus controls using radial 3DCT imaging and volumetric segmentation. Br J Radiol 2020;93:20190039.
38. Audenaert EA, Mahieu P, Pattyn C. Three-dimensional assessment of cam engagement in femoroacetabular impingement. Arthroscopy 2011;27:167-71.
39. Kang RW, Yanke AB, Espinoza Orias AA, Inoue N, Nho SJ. Emerging ideas: Novel 3-D quantification and classification of cam lesions in patients with femoroacetabular impingement. Clin Orthop Relat Res 2013;471:358-62.
40. Yanke AB, Khair MM, Stanley R, Walton D, Lee S, Bush-Joseph CA, Espinoza Orías A, Inoue N, Nho SJ. Sex Differences in Patients With CAM Deformities With Femoroacetabular Impingement: 3-Dimensional Computed Tomographic Quantification. Arthroscopy 2015;31:2301-6.
41. Guidetti M, Malloy P, Alter TD, Newhouse AC, Espinoza Orías AA, Inoue N, Nho SJ. MRI-- and CT--based metrics for the quantification of arthroscopic bone resections in femoroacetabular impingement syndrome. J Orthop Res 2022;40:1174-81.
42. Treece GM, Poole KE, Gee AH. Imaging the femoral cortex: thickness, density and mass from clinical CT. Med Image Anal 2012;16:952-65.
43. Mannava S, Geeslin AG, Frangiamore SJ, Cinque ME, Geeslin MG, Chahla J, Philippon MJ. Comprehensive Clinical Evaluation of Femoroacetabular Impingement: Part 2, Plain Radiography. Arthrosc Tech 2017;6:e2003-9.
44. Neubert A, Wilson KJ, Engstrom C, Surowiec RK, Paproki A, Johnson N, Crozier S, Fripp J, Ho CP. Comparison of 3D bone models of the knee joint derived from CT and 3T MR imaging. Eur J Radiol 2017;93:178-84.

Cite this article as: Bugeja JM, Xia Y, Chandra SS, Murphy NJ, Eyles J, Spiers L, Crozier S, Hunter DJ, Fripp J, Engstrom C. Automated volumetric and statistical shape assessment of cam-type morphology of the femoral head-neck region from clinical 3D magnetic resonance images. Quant Imaging Med Surg 2022;12(10):4924-4941. doi: 10.21037/qims-22-332

Supplementary

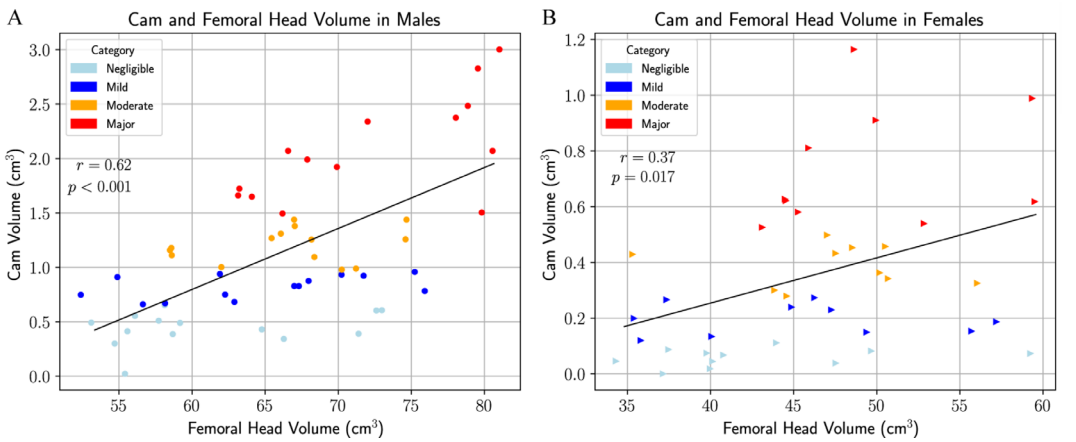

Figure S1 Correlation between femoral head volume and cam morphology volume in male (A) and female (B) patients.

Table S1 Comparison of the present study with related works on the proximal femur, femoral head, and hip joint segmentation in magnetic resonance imaging data

Study	Segmentation description	Subjects	MRI strength (T)	Average DSI
(13)	Proximal femur: multi-atlas method in 3D	30	3.0	0.95
(13)	Proximal femur: active shape models in 3D	30	3.0	0.946
(14)	Femoral head bone: focused shape models in 3D	25	3.0	0.98
(34)	Proximal femur: parametric deformable model in 3D (Dataset 1)	1	3.0	0.883
(34)	Proximal femur: parametric deformable model in 3D (Dataset 2)	1	3.0	0.883
(30)	Proximal femur: 3D U-net	20	–	0.987
(29)	Proximal femur: 2D and 3D U-net	86	3.0	0.95
(25)	Proximal femur: multi-level latent shape space constrained 3D U-net	25	–	0.954
(26)	Proximal femur: 3D U-net	20 (images)	–	0.987
(35)	Proximal femur: deep volumetric shape learning in 3D	24	–	0.933
(31)	Proximal femur: 3D tiled convolution in 3D	25 (images)	–	0.9814
(32)	Proximal femur: holistic decomposition convolution in 3D	25 (images)	–	0.9814
(33)	Proximal femur: random forest classifier with deformable model registration	25	1.5	0.9637
(36)	Proximal femur: deep segmentation in 2D U-net	6	1.5	0.8694
(36)	Proximal femur: deep segmentation in 2D Ref-Net	6	1.5	0.8617
(28)	Proximal femur: 2D CNN	13	1.5	0.8973
(27)	Femur bone: Resnet50-segnet	38	1.5	0.907
Our network	Proximal femur: 3D U-net	97	3.0	
U-net results				0.958
U-net + FSM results				0.964

FSM, focused shape model; 3D, three-dimensional; 2D, two-dimensional; CNN, convolutional neural network; MRI, magnetic resonance imaging; DSI, Dice similarity index.

https://dx.doi.org/10.21037/qims-22-332

Table S2 Comparison of the cam morphology quantification results with related works

Study	Method description	N	Image modality	μ volume (σ) (cm^3)	Volume range (cm^3)	μ SA (σ) (cm^2)	μ height (σ) (mm)	Max height (σ) (mm)
(38)	Mimics segmentation; femoral head and neck radii constraints	7 (M)	CT	–	–	3.735 (1.547)	–	–
(39)	Mimics segmentation; femoral head radii constraints	5	CT	–	–	–	SNS: 8.26	–
(10) FAI results	Manual segmentation; estimation of normal surface	5	3T MRI	SNS: 0.188 (0.247)	–	SNS: 0.52 (0.60)	SNS: 3.9 (2.1)	–
(40)	Mimics segmentation; femoral head radii constraints	M:F 69:69	CT	M: 0.433 (0.471); F: 0.089 (0.124)	–	–	M: 1.51 (0.75); F: 0.66 (0.61)	–
(45)	Region growing segmentation	M:F 20:23	CT	M: 6.7 (2.5); F: 4.3 (3.4)	1.2–12.5	–	–	–
(9)	Region growing segmentation	M:F 13:14	CT	SNS: 4.6 (2.6)	–	–	–	–
(37) abnormal FAI results	Region growing segmentation	79	CT	SNS: 7.96 (2.78)	–	–	–	–
(41) MR results	Mimics segmentation	7	CT and MRI	SNS: 0.940 (0.537)	–	SNS: 6.158 (2.324)	SNS: 1.6 (0.4)	SNS: 3.7 (0.9)
Ours	3D U-net and FSM	M:F 56:41	3T MRI	M: 1.136 (0.659); F: 0.338 (0.280)	M: 0.022–3.002; F: 0–1.164	M: 6.574 (2.030); F: 3.069 (1.756)	M: 1.94 (0.86); F: 1.00 (0.57)	M: 3.89 (1.51); F: 2.23 (1.09)

FAI, femoroacetabular impingement; MR, magnetic resonance; 3D, three-dimensional; FSM, focused shape model; M, male; F, female; CT, computed tomography; MRI, magnetic resonance imaging; μ, mean; σ, standard deviation; SNS, sex not specified; SA, surface area.

Table S3 Comparison of the femoral head volume results with related works

Study	Method description	Subjects	Image modality	μ volume (σ) (cm^3)			Volume range (cm^3)	μ radii (σ) (mm)
				Male	Female	Sex not specified		
(40)	Mimics segmentation; manual femoral head centre initialization; iterative search: σ to point cloud minimization	M:F 69:69	CT	–	–	–	–	M: 25.4 (1.3); F: 22 (1.3)
(45)	Region growing segmentation	M:F 20:23	CT	62.9 (10.8)	41.8 (8.6)	–	24.4–85.2	–
(9)	Region growing segmentation	M:F 13:14	CT	–	–	49.7 (11.5)	–	–
(37) abnormal FAI results	Region growing segmentation	79	CT	–	–	47.84 (9.65)	–	–
(21)	Manual analysis	M:F 44:53	1.5T MRA	57.16 (9.71)	37.98 (5.71)	–	–	–
(22)	Cadaveric measurements	1,090 hips	–	–	–	58.194 (11.998)	–	–
Ours	3D U-net, Hough transform, spherical fitting	97	3T MRI	66.12 (7.67)	46.02 (6.83)	–	M: 52.39–81.03; F: 34.31–59.49	–

FAI, femoroacetabular impingement; σ, standard deviation; 3D, three-dimensional; M, male; F, female; CT, computed tomography; MRA, magnetic resonance arthrography; MRI, magnetic resonance imaging; μ, mean;

https://dx.doi.org/10.21037/qims-22-332